Boron nitride formation on magnesium studied by *ab initio* calculations

S. Riikonen,[1] A. S. Foster,[1,2] A. V. Krasheninnikov,[1,3] and R. M. Nieminen[1,*]
[1]*COMP/Department of Applied Physics, School of Science and Technology, Aalto University, P.O. Box 11000, FI-00076 Aalto, Espoo, Finland*
[2]*Department of Physics, Tampere University of Technology (TUT), P.O. Box 692, FI-33101 Tampere, Finland*
[3]*Materials Physics Division, University of Helsinki, P.O. Box 43, FI-00014 Helsinki, Finland*
(Received 28 December 2009; revised manuscript received 10 March 2010; published 31 March 2010)

Motivated by the state of the art method for producing boron nitride nanotubes in which magnesium has been speculated to act as a catalyst, we study the elemental chemistry of boron and nitrogen on the Mg(0001) surface using *ab initio* methods. We do this by considering the energetics of individual boron and nitrogen atoms, and the smallest boron and nitrogen containing molecules. We observe that magnesium promotes boron-nitride (BN) molecule formation on the catalyst surface. Based on the analysis of the behavior of BN molecules on the catalyst surface, we propose a possible route for further development of hexagonal BN sheets mediated by the catalyst

DOI: 10.1103/PhysRevB.81.125442 PACS number(s): 36.40.Jn, 31.15.ae, 34.50.Lf, 75.50.Bb

I. INTRODUCTION

The boron-nitride nanotube[1–3] (BNNT) is a structural analogy of the more well-known carbon nanotube (CNT). Instead of a graphitic sheet made of carbon atoms only, the structure of BNNT consists of alternating nitrogen and boron atoms. The structure of BNNT then features the more ionic boron-nitrogen bond, which gives the BNNTs various promising physical properties. BNNTs are always semiconducting and the electronic gap in BNNTs (~5.5 eV) is practically independent of the nanotube chirality and its diameter.[4,5] BNNTs possess similar impressive mechanical properties as CNTs. Hexagonal boron nitride is also known to be very resistant to oxidation and for this reason, BNNTs have been proposed for shielding and coating applications at the nanoscale.[6] They also have high thermal stability and promising optical properties at the ultraviolet regime.[7]

Despite these and many other technological prospects,[7] BNNTs have received very little attention compared to CNTs due to various difficulties in their reproducible and efficient synthesis.[7] The methods to produce BNNTs, include the arc discharge, laser ablation, thermal annealing, and chemical-vapor deposition (CVD) synthesis (see Ref. 8 for an overview). Most of the experimental methods proposed up to date, show traces of catalytic particles in the fabricated materials but the role that these metal particles play in the BNNT synthesis is not well understood.[8] Moreover, in most of the methods, the yield and the quality of the nanotubes are poor. Similar to the case of CNTs, it would be very desirable to find an efficient CVD synthesis method for producing BNNTs. Unfortunately, BNNT synthesis using CVD and the traditional transition-metal catalysts has not been successful. Some success has been obtained using borides as catalysts (borides are able to dissolve boron and nitrogen simultaneously[9]). However, when using borides the situation becomes quite complex, as during the nanotube growth, the boron seems to come from the catalyst particle itself, instead of the CVD precursors.[9–11]

In an effort to understand the problems that might occur when using CVD with traditional transition-metal catalysts, we studied in an earlier work the elemental reactions of boron and nitrogen on an iron catalyst[8] and the energetics of N_2, B_2, and BN formation. Looking at this simplified situation, we observed that BN molecules (which are a likely prerequisite for further boron nitride formation) are stabilized only at special step-edge sites. In the present work we use a similar scheme and study boron-nitride chemistry on magnesium.

Magnesium has been speculated to act as a catalyst in the state of the art method of Golberg *et al.*,[7] Tang *et al.*,[12] and Zhi *et al.*,[13] for producing mass quantities of BNNTs. The details of this synthesis method are not fully understood, as the chemistry involved is rather complicated (see below Sec. II). However, magnesium seems to play an important role in the synthesis and in order to shed some light on the underlying boron-nitrogen-magnesium chemistry, we study this subject using the *ab initio* methods. Also from a purely theoretical point of view, magnesium as a catalyst metal is an interesting subject as its electronic structure is very different when compared to the more conventional transition metal catalysts. Some earlier *ab initio* investigations concerning adsorbates on magnesium have concentrated on the ability of magnesium to break the hydrogen bond and to store atomic hydrogen.[14–17]

This work is organized as follows: In Sec. II we first consider in detail the present state of the art method for producing BNNTs and then explain our strategy for studying boron-nitride chemistry on magnesium. Technical details are discussed in Sec. III with a systematic study of the interlayer relaxations in Mg(0001) slab and tests of the convergence of adsorption energies as function of the number of layers in the slab. After this, in Sec. IV, the adsorption geometries, energies, reaction energies, and reaction barriers for forming the simplest molecules of boron and nitrogen on magnesium are presented. Discussion and conclusions are made in Sec. V.

II. SYNTHESIS OF BNNTs

The synthesis method elaborated by Golberg *et al.*,[7] Tang *et al.*,[12] and Zhi *et al.*,[13] starts by producing Mg and B_2O_2

vapors from boron and MgO powders.[18] These vapors are then transformed to a reaction chamber where they are mixed with NH_3.[12] Magnesium is thought to act as a catalyst in the reduction in boric oxide into boron nitride.[12] In more detail, the reaction happens in two steps as follows:[12]

$$2B(s) + 2MgO(s) \rightarrow B_2O_2 + 2Mg, \quad (1)$$

$$B_2O_2 + 2NH_3 \rightarrow 2BN(s) + 2H_2O + H_2. \quad (2)$$

Reactions take place in the gas phase while the precursors and the final product are in the solid state [marked with (s)] and liquid magnesium droplets act as catalysts[7,12,13,19] in the second line of this reaction. The temperature gradient in the reaction chamber is high and it has been estimated that at the chamber walls where the tubes are formed, temperature is in the range of 800–850 °C.[20] In their original paper Tang *et al.*[21] proposed that liquid magnesium might act as a catalyst for BN formation, an explanation that has been used in successive works.[7,13,19] These presumed catalyst droplets become eventually poisoned as they form $Mg_2B_2O_5$,[13] a problem that can be solved by adding iron to the catalyst.[13]

We can try to get some insight into this complex situation from a thermodynamical database.[22] The driving force for nanotube formation comes from going toward thermodynamical equilibrium for Mg, B_2O_2, and NH_3 at ~800 C°. At $T \sim 800$ C° and at atmospheric pressures, one gets typically considerable amounts of boron nitride, magnesium oxide, hydrogen, and magnesium-boron-oxide compounds.[22] Thermodynamical data then suggests that boron nitride is always formed in considerable quantities, which is in accordance with the experiment. The appearance of magnesium-boron-oxygen compounds manifests the tendency of magnesium to form oxides and borides.

From the experiments, an interesting observation is that when iron is added to the reaction,[13] the nanoparticles that are sometimes found encapsulated at the end of the nanotubes, consist solely of magnesium and iron.[13] Then, either the pure catalyst nanoparticle interpretation is the correct one or the nanocluster that originally contained magnesium, iron, borides, and oxides is completely reduced from boron, nitrogen, and oxygen as the BNNT is formed.

Concluding, whatever the exact mechanism for boron-nitride nanotube formation is (magnesium droplets acting as catalyst particles, reduction in more complex clusters into magnesium, and BN), in order to better understand this synthesis method it is important to understand the underlying boron-nitrogen-magnesium chemistry, a subject that to our knowledge has not been addressed with *ab initio* calculations.

We study this subject by adsorbing individual B and N atoms on the Mg(0001) surface and calculate the reaction energetics and barriers as these adsorbed atoms (X^* and Y^*) form adsorbed molecular species (XY^*) on the surface. The cases we consider are $X^*=N^*$ and B^*, and $XY^*=N_2^*$, B_2^*, and BN^*, i.e., the individual atoms and the most simple molecules.

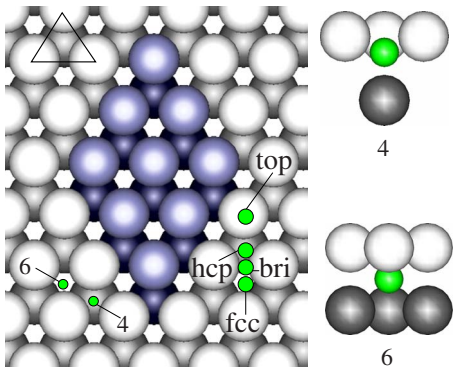

FIG. 1. (Color online) Magnesium Mg(0001) surface. The top layer and the layer below are marked with lighter and darker shades, respectively. The unit cell used in this study is marked with blue color. The unit cell side is ≈9.6 Å long and it corresponds to a 3×3 periodicity. One side of the triangle connecting nearest neighbors in the topmost layer is 3.19 Å. Some special adsorption sites in the Mg(0001) are marked as follows: top, hcp, bri (bridge), and fcc. The fourfold tetragonal site is marked with "4" and the sixfold octahedral site with "6." The tetragonal and octahedral sites are also illustrated from side at the rightmost panels. Distance from the tetragonal and octahedral sites to the surrounding Mg atoms are ≈2.0 and 2.3 Å, respectively.

III. METHODS

A. Technical details

As described in the previous section, we concentrate in calculating reaction energies and barriers for reactions $X^*+Y^* \rightarrow XY^*$ on the catalyst surface using slabs. Molecules are adsorbed in the unit cell of a periodic surface slab and vacuum between slabs is always >14 Å. The Mg(0001) surface together with the unit cell used in our calculations is depicted in Fig. 1.

We assume that two adsorbates, X^* and Y^*, are far away from each other on the surface and we bring them together to form a new adsorbate species XY^*. The energy for this reaction $X^*+Y^* \rightarrow XY^*$ can be calculated as follows:

$$\Delta E = [E(XY^*) + E_0] - [E(X^*) + E(Y^*)], \quad (3)$$

where $E(X^*)$ is the energy of the adsorbed surface species X^* and E_0 is the energy of a surface unit cell without adsorbates. This equation can be written in a more convenient form

$$\Delta E = E_s(XY^*) - [E_s(X^*) + E_s(Y^*)]. \quad (4)$$

Where we have defined energy values E_s as

$$E_s(X^*) = E(X^*) - E_0. \quad (5)$$

In the results section, we tabulate values of E_s and then use these tabulated values to calculate reaction energetics $X^*+Y^* \rightarrow XY^*$ using Eq. (4). Using the same notation, the adsorption energy can be written as follows:

$$E_{ads} = E(X^*) - E(X) - E_0 = E_s(X^*) - E(X). \quad (6)$$

The calculations were performed in the framework of the density-functional theory (DFT), as implemented in two different codes, SIESTA and VASP. The SIESTA code[23,24] uses

pseudoatomic orbitals as its basis set while VASP (Refs. 25–27) is based on plane waves. SIESTA relies on the pseudopotential method to describe the core electrons while projected augmented waves (PAWs) (Ref. 28) can be used in VASP. All calculations were done using the Perdew-Burke-Ernzerhof (PBE) general gradient approximation[29] exchange-correlation (XC) functional. Some test calculations were also performed using the revPBE XC functional.[30] We used the Monkhorst-Pack (MP) sampling[31] of the Brillouin zone in calculations involving the slab. For the 3×3 slab, a 7×7 MP sampling was used. This corresponds to $A_{BZ}=0.01$ Å^{-2} (area in the reciprocal space per sampled k point) and the same A_{BZ} value was used with different surface slabs. A systematic search to find the optimal adsorption sites for nitrogen, boron and N_2, B_2, and NB molecules on the slab of Fig. 1 was performed along the lines of Ref. 8. During the search, some preliminary calculations were done with SIESTA while the final energies were always calculated with VASP.

Spin polarization was included when calculating individual atoms and molecules in vacuum. However, it was not included in calculations involving the slab; magnesium is not expected to be magnetic and spin polarization of molecules typically reduces upon adsorption. We also made a few test calculations including spin polarization for cases when atoms and molecules with uneven number of electrons are adsorbed on magnesium surface and observed no net spin.

In the SIESTA calculations, a SZSP basis with 150 meV energy shift defining the cut-off radii for orbitals was used for all atomic species. This way magnesium $3s$ and $3p$ orbitals obtain cut-off radii of 3.8 Å (see Ref. 8 for more details). In VASP, PAWs were used. The cut-off energy of the plane-wave-basis set was always 420 eV. Mixing scheme in the electronic relaxation was the Methfessel-Paxton method[32] of order 1. Conjugate gradient relaxation of the geometry was performed and if needed, the relaxation was continued with a semi-Newton scheme. This way we were able to reach a maximum force residual of ≈0.02 eV/Å. In all calculations special Davidson block iteration scheme was used and symmetries of the adsorption geometries were not utilized. The standard "normal" accuracy was used.

Nudged elastic-band (NEB) calculations[33] were performed with VASP. Atoms in the topmost layer were allowed to move freely while atoms below the topmost layer were allowed to move into z direction (normal to the surface slab) only. In some cases a similar condition was applied to some atoms in the topmost layer as well. This way we were able to avoid the (artificial) collective movement of the surface slab atoms that sometimes occurred during the minimizations.

B. Bulk magnesium

We first checked that bulk magnesium, calculated with SIESTA and VASP, gave consistent results. The experimental value for bulk magnesium lattice constant are $a=3.21$ Å and $c=5.21$ Å.[34] When optimizing the computational lattice constant, we observed that the ratio c/a was always equal to the experimental value of 1.62.[35,36] For SIESTA we then obtained the value $c=5.32$ Å while for VASP we calculated $c=5.18$ Å with the PBE XC functional and $c=5.21$ Å with the revPBE XC functional. The band structure as calculated both with SIESTA and VASP was identical to an earlier theoretical result.[35]

C. Mg(0001) surface

The interlayer distances of the topmost layers in Mg(0001) are known to relax, the distance between the first two topmost layers expanding in the range of 1–2 % when compared to bulk values.[36,37] This behavior has been explained by Friedel oscillations that are formed at the bulk-vacuum interface.[37] These oscillations die out rapidly but in the topmost atomic layers they either accumulate or deplete charge, making the layers either repel or attract each other.[37]

As we are performing slab calculations, Friedel oscillations will form at both sides of the slab. If the slab is too thin, the decaying tail of these oscillations might affect the electron density in the opposite side of the slab. As the interlayer relaxations are coupled to these oscillations (as explained above), one might get incorrect distances between the topmost layers when using thin slabs, a behavior that could affect the adsorption energies. Talking in terms of individual one-electron states, Mg(0001) is known to have a resonantlike surface state with a tail that decays very slow into the bulk.[38,39] An artificial splitting of this surface state will be present in a slab calculation. This splitting has been observed in theoretical calculations[38] and in experiments measuring spectra of very thin magnesium slabs grown on tungsten.[39] It vanishes very slow as function of the slab thickness so rather big magnesium slabs should be used (>30 layers) in order to make the splitting vanishingly small.

In order to choose the correct strategy (slab thickness, fixed atoms, etc.) for making adsorption calculations on Mg(0001) we have first studied the delicate interlayer relaxations of Mg(0001) and plotted in Fig. 2 the distance between neighboring layers inside the slab. For the empty slab, two cases have been considered: either all atoms in the slab are allowed to relax or only the atoms in the three topmost layers are allowed to move while the atoms in the rest of the slab are fixed at their bulk positions. In the following discussion, we refer to the topmost layer as the layer number (1). Looking at the "free slab" case of Fig. 2, where no atoms have fixed positions, we observe that the distance between layers (1) and (2) converges to an expansion of $\sim1.5\%$ while the distance of layers (2) and (3) converges almost to the bulk value. Looking in more detail at interlayer distances of the free slab with $N=6$ layers, we get: +1.6%, +0.2%, −0.4%, and −0.2%. This compares very well with an earlier result obtained with local-density approximation:[37] +1.8%, +0.2%, −0.3%, and −0.1%. Relaxation patterns for a slab with only three topmost layers relaxing, are plotted in the left panel (three free layers) of Fig. 2. Fixing most of the atoms in the slab can have surprising effects in the topmost layers; this can be seen for example in the case $N=8$, where the interlayer distances between layers 2–4 are badly converged.

We can conclude that the interlayer relaxations depend on slab thickness and frozen layers and that fixing many layers may have surprising effects in the smallest slabs. On the

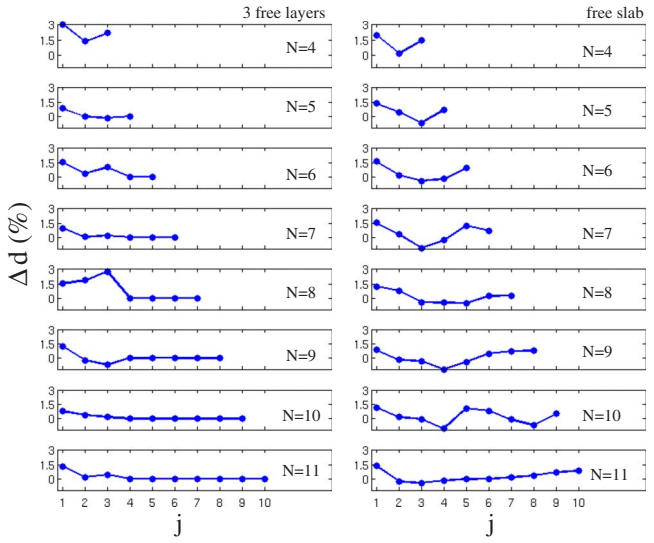

FIG. 2. (Color online) Interlayer relaxations in a 1×1 Mg(0001) slab: distances of layers (Δd) when compared to the bulk magnesium case. $\Delta d=1\%$ corresponds to an expansion of 26 mÅ between the layers. Distances between layers j and $j+1$ are plotted ($j=1$ being the topmost layer). The total number of layers (n) is indicated in the insets of the figures. Slabs consisting of 4 up to 11 Mg(0001) layers have been considered. Relaxation patterns, when the three topmost layers are allowed to move (left panel "three free layers") and when there are no fixed layers (right panel "free slab") have been plotted.

other hand, in the freely relaxed slab, calculations become time consuming as all the layers rearrange their z positions. From the point of view of adsorption energies, we are mainly interested in producing the correct behavior and interlayer distances in the topmost layers on only one side of the slab. We are also interested in making the Friedel oscillations coming from the opposite side of the slab small. For these purposes, only few relaxing layers in a sufficiently thick slab should result in convergent adsorption energies.

In Fig. 3 we have plotted the variation in the adsorption energy of geometry (N-2) (see Fig. 4) as function of number of magnesium layers. The calculations were performed by adsorbing the nitrogen atom into a 2×2 unit cell. Both

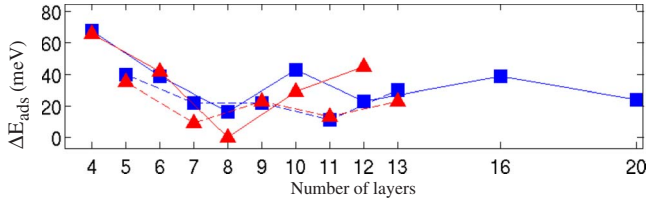

FIG. 3. (Color online) Variation in adsorption energies (ΔE_{ads}) for adsorbate N-2 (see Fig. 4) as a function of the number of magnesium layers in a 2×2 slab. Two different simulations setups are considered: either only atoms in three topmost layers are allowed to move (blue squares) or all atoms in the slab are free to move (red triangles). Lines connecting the energy values in order to guide the eye have been plotted: values corresponding to even-numbered layers are marked with a solid line while values corresponding to odd number of layers are marked with a dashed line.

cases, where the slab has either no fixed atoms or when only three layers are allowed to relax, have been considered. The oscillation in energy as function of slab thickness is seen to behave better for odd numbered layers. For odd numbered layers the two different slabs (either no fixed atoms or only three relaxing layers) give also more consistent results. According to Fig. 3, by using a nine-layer slab, with three freely relaxing layers, we are able to reach an accuracy of ~20 meV in the adsorption energies. For the calculations done in the remaining part of this work, we chose a slab consisting of a 3×3 unit cell and nine layers. Again, three of the topmost magnesium layers are allowed to relax while the rest of the magnesium atoms are fixed at their bulk positions. The slab can then be described as "$3\times3\times9$" and it contains 81 magnesium atoms.

IV. RESULTS

As we explained in previous sections, we concentrate on the most simple molecules that can be formed from N^* and B^* that are adsorbed on the catalyst surface and look directly at the energetic balance of the reactions $X^*+Y^*\rightarrow XY^*$ that form BN^*, N_2^*, and B_2^*. When calculating the reaction energies, we use Eq. (4) and tabulated values of E_s.

The optimal positions for adsorbed N, B, N_2, B_2, and BN are illustrated in Fig. 4. The indices given to these molecular geometries (B_2-1, B_2-2, etc.) are the same as used in Tables I and II and in the density of state plots in Figs. 6–8. The reaction energetics on the magnesium slab is summarized in Table II. From Table II, the most interesting result is, that on the contrary to iron,[8] the BN molecule is stabilized on magnesium.

Some test calculations, in order to see how our results depend on the PBE and revPBE XC functionals have also been performed. The difference of adsorption energies when calculated with these two different XC functionals have been tabulated in Table I. One can observe that revPBE gives systematically higher adsorption energies by 5–8 % (i.e., the molecule-substrate bonding becomes less favorable). The biggest effect is obtained for the N_2 molecule, where the relative change in the adsorption energy is ~50%. However, this is not a surprise as the molecule-substrate bond in the N_2 case is extremely weak. This special case has been discussed in the following sections in more detail and it does not affect our qualitative results (the N_2 adsorption energy merely changes from −0.02 to −0.01 eV, i.e., it is practically zero). Before analyzing the electronic structure of the adsorbates (Sec. IV B), reaction barriers (Sec. IV C) and a possible path for further BN formation (Sec. IV D) we will perform a detailed analysis of the adsorption geometries of Fig. 4.

A. Adsorption energies and geometries

As can be seen from Table I and Fig. 4, both nitrogen (N-1) and boron (B-1) atoms prefer the sixfold octahedral site. While searching for the optimal adsorption sites of the atoms, we observed that boron relaxed always spontaneously to the sixfold site (B-1), while nitrogen, depending on the initial position on the surface, relaxed either to the sixfold

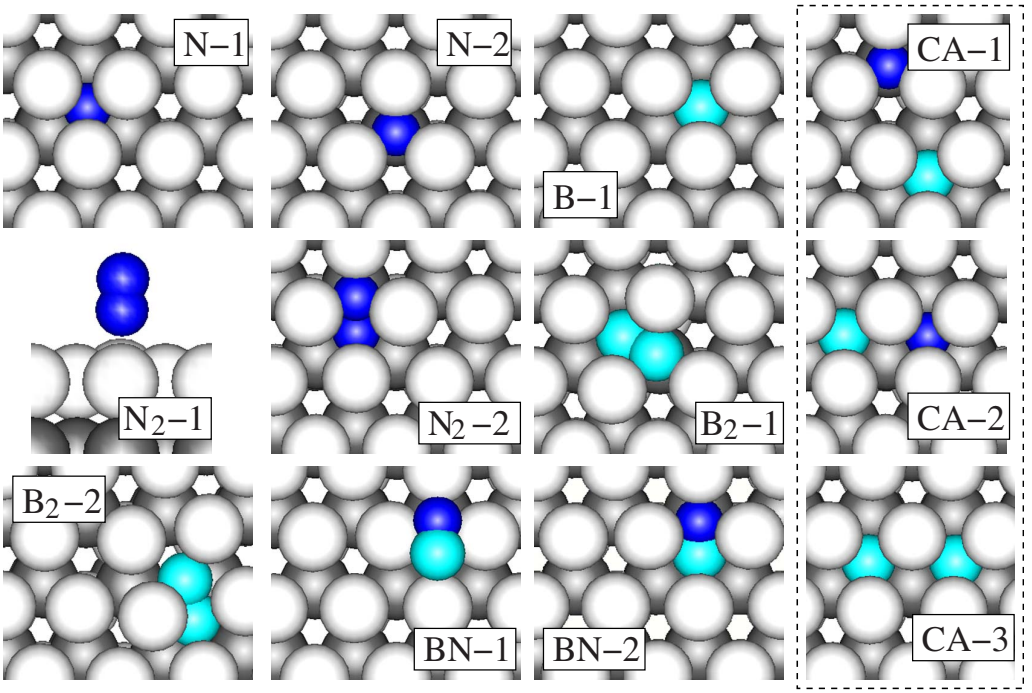

FIG. 4. (Color online) Some of the most stable geometries for B_2, BN, and N_2 molecules and the B and N atoms on the Mg(0001) surface. Different geometries are tagged with the same labels as in Table I. In the case of BN, magenta (blue) corresponds to boron (nitrogen). Some coadsorption geometries, where atoms are adsorbed into the same unit cell are tagged with the label CA.

(N-1) or the fourfold (N-2) site. As can be seen from Table I these adsorption geometries are energetically quite close to each other, N-1 being 0.23 eV more favorable than N-2. As will be discussed in the following section, there is a migration barrier between configurations N-1 and N-2.

In the adsorption geometry N-1 the nitrogen atom is surrounded by six magnesium atoms and the N-Mg distances are 2.16–2.18 Å. In the case of boron atom (B-1) the B-Mg distances are slightly bigger, ranging from 2.30 to 2.35 Å.

TABLE I. Adsorption energies E_{ads} and energies E_s [see Eq. (5)]. Values of E_s can be used directly to calculate reaction energies on the surface by using Eq. (4). Values for N_2, BN, and B_2 molecules, and N and B atoms in different adsorption geometries on the Mg(0001) surface have been tabulated. Bond lengths (BL) on the adsorbant and in the vacuum (in parenthesis) are listed. Sites and geometries have the same labels as in Figs. 4–8 and in Table II. Coadsorption geometries are tagged with "CA." Energy values in parenthesis show the energy difference when the system has been calculated with revPBE instead of the PBE XC functional ($E_{ads}^{revPBE}-E_{ads}^{PBE}$).

Adsorbate	E_{ads} (eV)	E_s (eV)	BL (Å)
N-1	−6.19 (0.49)	−9.31	
N-2	−5.96	−9.08	
B-1	−5.09 (0.28)	−5.38	
N_2-1	−0.02 (0.01)	−16.64	1.13 (1.12)
N_2-2	0.06	−16.55	1.6
B_2-1	−7.02 (0.39)	−11.26	1.57 (1.62)
B_2-2	−6.99	−11.24	1.584
BN-1	−6.57 (0.33)	−15.31	1.32 (1.33)
BN-2	−6.52	−15.27	1.414
CA-1		−14.32	
CA-2		−14.81	
CA-3		−10.55	

TABLE II. Reaction energies (eV) of some reactions on the magnesium surface. The adsorbate geometries that are used to calculate the energy for reaction $X^*+Y^* \rightarrow XY^*$ are indicated in parenthesis. Geometries are tagged with the same labels (N-1, N-2, etc.) as in Table I and Fig. 4. Reaction energies are calculated by taking the corresponding energies E_s from Table I and using Eq. (4).

Reaction		ΔE
$2B^* \rightarrow B_2^*$	[2(B-1) → B_2-1]	−0.51
$B^*+N^* \rightarrow BN^*$	[(B-1)+(N-1) → BN-1]	−0.62
$2N^* \rightarrow N_2^*$	[2(N-1) → N_2-1]	1.99
$B^*+N^* \rightarrow BN^*$	[(B-1)+(N-2) → BN-1]	−0.86
$B^*+N^* \rightarrow BN^*$	[(B-1)+(N-1) → BN-2]	−0.58
$2N^* \rightarrow N_2^*$	[(N-1)+(N-2) → N_2-1]	1.76
$B^*+N^* \rightarrow BN^*$	(CA-1 → BN-1)	−1.00
$B^*+N^* \rightarrow BN^*$	(CA-2 → BN-1)	−0.51
$B^*+N^* \rightarrow BN^*$	(CA-2 → BN-2)	−0.45
$2B^* \rightarrow B_2^*$	(CA-3 → B_2-1)	−0.72
$B^*+N^* \rightarrow B^*+N^*$	[(B-1)+(N-1) → CA-2]	−0.12
$B^*+N^* \rightarrow B^*+N^*$	[(B-1)+(N-1) → CA-1]	0.37
$B^*+N^* \rightarrow B^*+N^*$	(CA-1 → CA-2)	−0.49
$2B^* \rightarrow 2B^*$	[2(B-1) → CA-3]	0.21

The bigger distances seem natural as boron has more extended orbital radii than nitrogen. We can conclude that both nitrogen and boron prefer the most spacious site with highest coordination. In the metastable adsorption geometry N-2, the nitrogen atom is in the fourfold tetrahedral site, surrounded by four magnesium atoms, all at the distance of ≈2.00 Å (N-Mg distances being ~7% smaller than in N-1).

The adsorption of N_2 on magnesium is not energetically feasible; for the standing position geometry N_2-1, the adsorption energy is practically zero while for N_2-2 it is positive. This implies that N_2 is probably not a good N-carrying precursor when using a magnesium catalyst. The standing position N_2-1 has a minimal interaction with the surface while N_2-2 can be understood in terms of adsorption sites of individual nitrogen atoms: nitrogen atoms are accommodating the two most favorable sites available for them, i.e., adsorption geometries N-1 and N-2. However, while doing this, the N-N bond length becomes quite large and is expanded by ~40%, so the molecule is almost dissociated. We also observed a significant change in the geometry when relaxing the N_2-1 adsorbate using the revPBE XC functional instead: with PBE, the N-Mg distance is 2.4 Å, while using revPBE, N_2 moves further away from the surface and the distance becomes 3.76 Å. Bonding of N_2 molecule with the magnesium substrate in the N_2-1 adsorption geometry is very weak (see Sec. IV B). In this kind of case we might expect very different behavior from the PBE and revPBE functionals, as PBE is known to exaggerate the adsorption and bond-formation energies.[40,41]

The adsorption geometries B_2-1 and BN-2 can be understood in terms of adsorption of individual nitrogen and boron atoms: in adsorbate B_2-1, one of the boron atoms is at the favorable octahedral (B-1) site while the other one is accommodated in the tetrahedral site. This way the B_2 molecule can maintain a reasonable bond length (contracted only by 3% from the free molecule case) while keeping at least one of the atoms in the octahedral (B-1) site. BN-2 can be understood exactly in the same terms, i.e., by keeping in mind the optimal adsorption sites of the individual atoms. Now boron is occupying the site most favorable for an individual boron atom (B-1) while nitrogen occupies the "second best" option for an individual nitrogen atom, the metastable site (N-2). BN bond length is expanded only 6% from the isolated molecule case.

Finally, the most favorable adsorption geometry for boron nitride, BN-1, cannot be explained in terms of the B-1, N-1, and N-2 adsorption geometries; instead of accommodating sites similar to individual atoms, the molecule adsorbs above the topmost surface layer. Keeping in mind Fig. 1, adsorption geometry BN-1 can be described as N atom residing at the "hcp" and B at the "fcc" site. Interestingly, the B-N bond length is almost identical to the isolated molecule case (less than one per cent contraction). The molecular axis is slightly inclined, the nitrogen atom being closer to the surface than the boron atom. The N-Mg distances are in the range 2.10–2.20 Å while the B-Mg distances in the range 2.36–2.39 Å. In order to further analyze this adsorption geometry, we have visualized the charge transfer between the molecule and the substrate in Fig. 5. From Fig. 5 we can observe charge transfer to the bonding-type σ_{pz} orbital. The

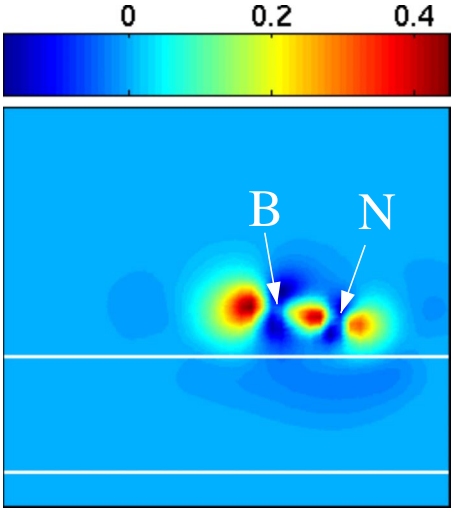

FIG. 5. (Color online) Intensity plot for charge distribution ρ (*surface and molecule*)-ρ (*surface*)-ρ(*molecule*), where $\rho(x)$ denotes the self-consistent charge distribution of either the isolated system (x=surface or x=molecule) or the composite system (x=surface and molecule). The plotting plane encloses the molecule axis and Mg(0001) planes are indicated with white lines. Positive values indicate accumulation of electrons. The plot corresponds to the adsorption geometry BN-1 of Fig. 4.

situation can then be described as BN molecule ionizing the magnesium surface and transferring charge to the σ_{pz} orbital. We tried also to stabilize a similar geometry for the B_2 molecule without success; the adsorption geometry BN-1 then seems to be unique for the BN molecule. We also found a degenerate adsorption geometry; BN at the BN-1 geometry can be turned around 180 degrees, i.e., putting N at the fcc and B at the hcp sites instead. This rotated BN molecule has the same adsorption energy as the original BN-1 adsorbate.

Adsorption geometry BN-1 is very suggestive for further boron-nitride nucleation; if we fill the surface with BN molecules in the adsorption geometry BN-1, we obtain a periodic structure that starts to resemble very much a graphitic boron-nitride sheet. We have performed a test calculation for this kind of situation in Sec. IV D.

B. Electronic structure of adsorbates

In an earlier work,[8] we visualized the projected density of states of the adsorbant/adsorbate system for an iron catalyst and the molecules in question (B_2, N_2, and BN). The iron spectra are dominated by the *d* states while the magnesium spectra feature free-electronlike *s* states. The *s* states are known to have weak interaction with the adsorbate molecular states[40] and the peaks of the molecular states are typically broadened and no bonding/antibonding gaps are developed for a certain molecular state resulting from its interaction with the adsorbant.[42] In the case of magnesium, the *s* states dominate the spectra and they reach deeper in energy than the *s* states of iron. In order to see how the adsorbate molecular states align with the adsorbant density of states (without substrate-molecule bond formation), we have plotted in the insets of Figs. 6–8 the projected density of states (PDOS)

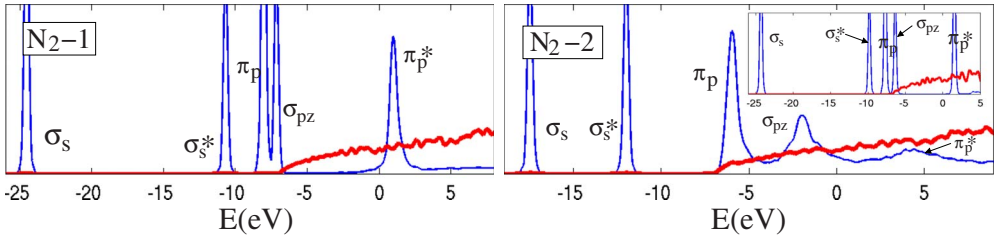

FIG. 6. (Color online) Density of states of adsorbed N_2 molecule and the Mg substrate, projected into atom-centered magnesium orbitals (thick red line) and into N atom centered s and p orbitals (blue line). The electronic states have been identified using the molecular orbital theory (see, for example, Ref. 8). Panels (N_2-1) and (N_2-2) refer to the surface geometries in Table I and in Fig. 4. In the inset of panel (N_2-2), the projected density of states for a situation where N_2 molecule is far away from the surface has been plotted. $E=0$ eV corresponds to the Fermi level.

in a situation where the molecule lies far away from the surface (distance 6.5 Å).

We start the analysis of the electronic structure by looking at the case of the N_2 molecule: from the inset in Fig. 6 we can see that magnesium s states should interact dominantly with the π_p^* state of N_2 molecule when the molecule is placed on the catalyst. Looking at the PDOS of adsorption geometries N_2-1 and N_2-2 in Fig. 6 we can see that this is the case; for N_2-1 there is only a slight charge transfer from the magnesium surface to the molecular π_p^* state (i.e., a slight downward shift and broadening of the π_p^* peak). The fact that magnesium interacts dominantly with the antibonding π_p^* orbital explains the instability of N_2-1 on the magnesium surface. For N_2-2 there seems to be a weak interaction with both π_p and σ_{pz} molecular states. The π_p^* peak has melted out completely, implying a strong hybridization of this state with magnesium. The gap between σ_s and σ_s^* has closed up from ~15 eV down to ~5 eV, implying that we are near molecular dissociation.

Looking at the case of B_2 adsorption and the inset of Fig. 7, we observe that magnesium states reach all the way down to the molecular σ_s^* antibonding state. Looking at the PDOS corresponding to adsorption geometry B_2-2 in Fig. 7, we observe that DOS peaks corresponding to σ_s^*, σ_{pz}, π_p, and π_p^* states have "melted out," i.e., they have a strong interaction with the magnesium substrate. Within the molecules considered here, B_2 seems to be the only one that bonds to the magnesium substrate using the antibonding σ_s^* orbital and this could have a destabilizing effect on the molecule (with respect to BN). Finally, looking at the case of the BN molecule in Fig. 8, we observe a strong interaction with the

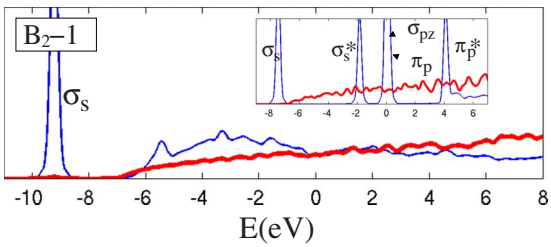

FIG. 7. (Color online) Density of states of adsorbed B_2 molecule and the Mg substrate, projected into atom-centered magnesium orbitals (thick red line) and into B atom centered s and p orbitals (blue line). For more details, see caption of Fig. 6.

antibonding π_p^* orbital and charge transfer (i.e., slightly smeared peaks that are shifted to negative energies) into the σ_{pz} and π_p orbitals. This charge transfer to the σ_{pz} orbital is consistent with Fig. 5.

C. Reaction energies and barriers

Looking at Table II, we can observe that N_2 formation from the dissociated precursors does not pose a problem. The situation for reactions $B^*+N^* \rightarrow BN^*$ and $B^*+B^* \rightarrow B_2^*$ is more subtle and these reactions are obviously competing. Looking at the first three rows of Table II we can see that BN forming reaction [(B-1)+(N-1)→BN-1] is ~100 meV more favorable than the B_2 forming reaction [2(B-1) →B_2-1] and this should be desirable for further BN formation. On the other hand, this value is at the accuracy limit of our calculations. The most interesting qualitative result is, however, that BN bond is stabilized on the magnesium surface (i.e., the reaction energy is clearly negative).

In reaction [(B-1)+(N-1)→BN-1] we assume that the adsorbed atoms are far away on the surface and we then bring them together to form a molecule. The reaction energetic changes considerably when we take as a starting point a coadsorbed configuration, where the B and N atoms are in the same unit cell to begin with, i.e., when considering the reaction (CA-2→BN-1) in Table II. When comparing reactions [(B-1)+(N-1)→BN-1] and (CA-2→BN-1), the energy is seen to change by 110 meV. The reason for this is, that by bringing the molecules to the same unit cell, i.e., the reaction [(B-1)+(N-1)→CA-2], already brings the energy down by 120 meV. In principle, the BN bond is then stabilized more than the B_2 bond but at high concentrations it seems that this tendency is reversed. On the other hand, it is energetically favorable to bring boron and nitrogen into neighboring sites and this might be desirable for BN nucleation. In Table II we have also considered BN molecule formation into the final adsorption geometry BN-1, when the initial position of the nitrogen atom is the metastable N-2 site [(B-1)+(N-2)→BN-1] and it implies that if the number of octahedral adsorption sites become scarce (as both nitrogen and boron prefer these sites) the BN molecule formation becomes very favorable.

In order to further understand the competition between the different reactions, we have studied the barriers for B and N atom diffusion and for the $B^*+B^* \rightarrow B_2^*$ and $B^*+N^* \rightarrow BN^*$

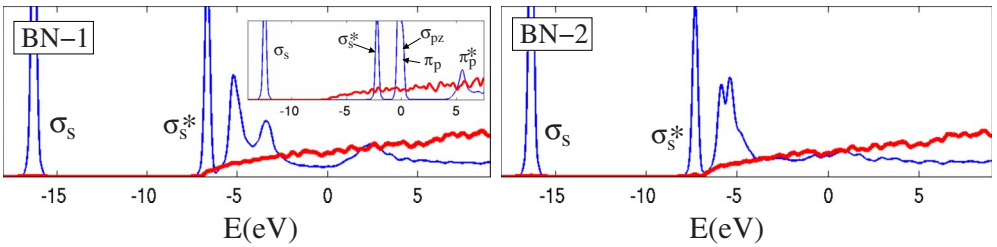

FIG. 8. (Color online) Density of states of adsorbed BN molecule and the Mg substrate, projected into atom-centered magnesium orbitals (thick red line) and into B and N atom centered *s* and *p* orbitals (blue line). For more details, see caption of Fig. 6.

dissociation/association reactions. Barriers and some atomic geometries along the minimum energy path have been illustrated in Figs. 9 and 10. The zero of energy has been adjusted in each of the graphs in order to make the comparison most convenient.

The N migration barrier in Fig. 9(a) is higher (0.94 eV) than the B migration barrier (0.72 eV) of Fig. 10(a). At the transition state, N atom is approx. threefold coordinated (to two Mg atoms at the topmost layer and to one Mg atom below). The transition state for B migration is very close to the tetrahedral adsorption site. Both B and N stay below the topmost surface layer during migration. One possible path for BN-1 dissociation/association is presented in Fig. 9(b); in the case of BN-1, the nitrogen atom is already very near to the metastable N-2 site, so BN-1 is dissociated most naturally to the CA-1 coadsorption configuration. During the NEB calculation on this pathway, the BN molecule spontaneously visits the BN-2 adsorption geometry (or to be more exact, a geometry that is very close to BN-2). In Fig. 9, the limiting barrier for a reaction where N moves first to the tetrahedral site [as illustrated in Fig. 9(a)] and from there forms a BN bond to the BN-1 configuration [Fig. 9(b)], is seen to be the N migration barrier (0.72 eV). The barrier from the coadsorption configuration CA-1 to BN-1 is 0.60 eV. Once the BN bond is formed, it is not that difficult to move between BN-1 and BN-2 (barrier of 0.56 eV) but the dissociation back to boron and nitrogen has a high barrier of 1.6 eV. The transition state of BN dissociation in Fig. 9(b) is similar to the transition state of B atom migration of Fig. 10.

Another pathway for forming BN is illustrated in Fig. 10(c); now the association barrier is 0.80 eV while dissociation back to boron and nitrogen has a barrier of 1.25 eV. Once at the BN-2 configuration, BN molecule could, of course, migrate again easily to the BN-1 configuration. The transition state for BN-2 dissociation/association is similar to the transition state of the N atom migration.

The situation for B_2 molecule in Fig. 10(b) is seen to be quite different from the other ones; the barrier is very low and for association it is only 0.25 eV while for dissociation it is 0.97 eV. These small barriers for B_2 association/dissociation reactions when compared to the BN reactions can be explained by the different nature of the minimum energy path. In Figs. 9(b) and 10(c), both the B and N atoms have to pass through transition states that are very similar to the transition states of the migration of individual B and N atoms. In the case of Fig. 10(b) and when dissociating the B atoms to the most favorable B adsorption sites (octahedral site), there is no need to pass through the transition state for B migration (tetrahedral site) and this seems to make the barrier for B_2 association/dissociation small.

Within these simple considerations (B_2 and BN molecules forming and breaking from their preferred adsorption sites) and for high activation energies (~1 eV), there seems to be a regime where both B_2 and BN molecules are formed but

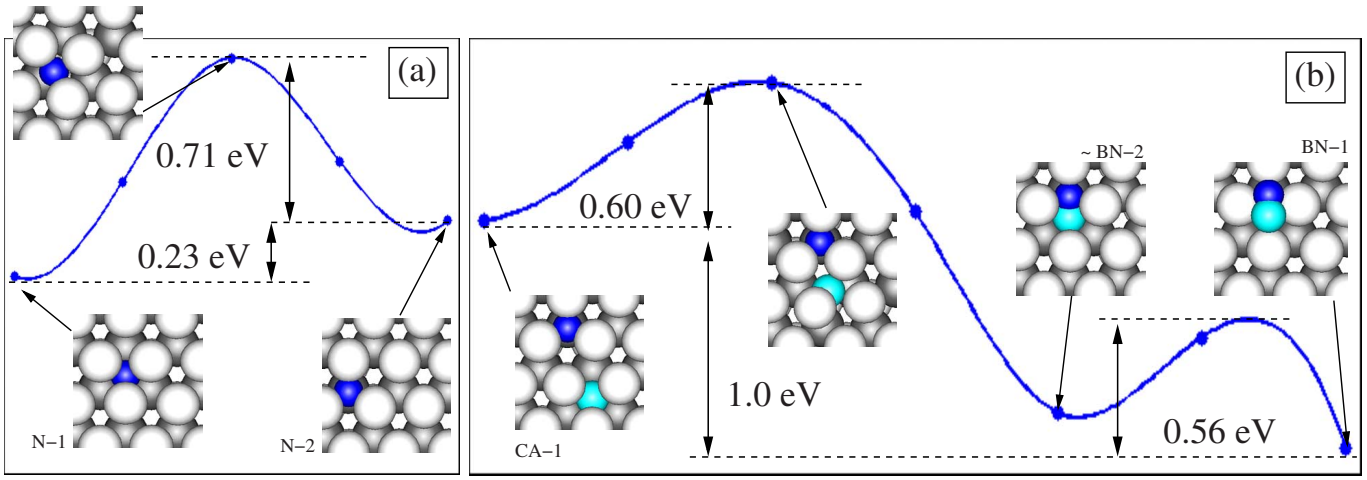

FIG. 9. (Color online) (a) Barrier for N diffusion (using three image points) and (b) BN association/dissociation reactions (with five image points) on the Mg(0001) surface as calculated with NEB. Atomic geometries along the minimum energy path have been illustrated in the insets.

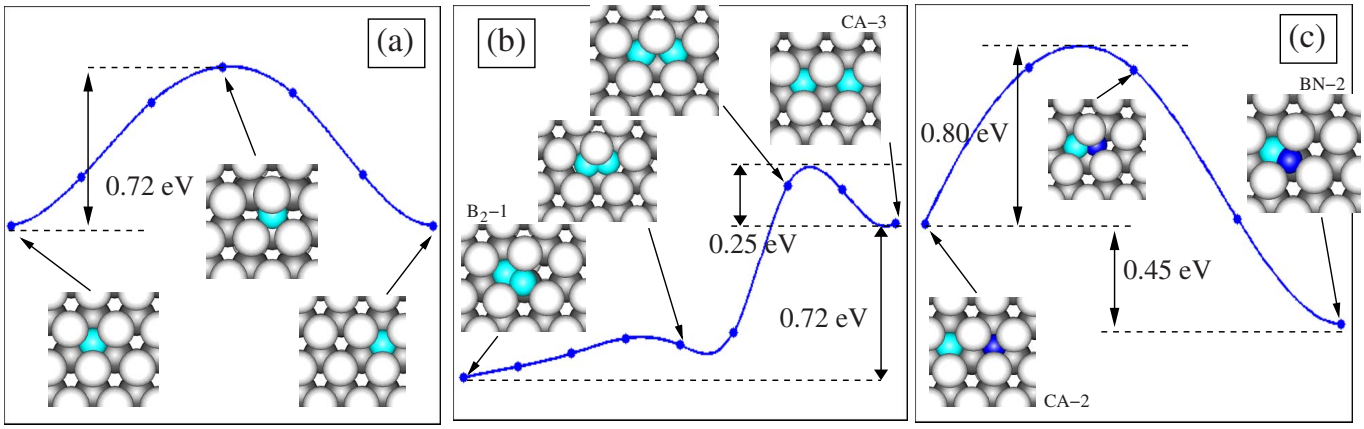

FIG. 10. (Color online) (a) Barrier for B diffusion (using five image points) and (b) B_2 (seven image points) and (c) BN association/dissociation reaction (three image points) on the Mg(0001) surface as calculated with NEB. Atomic geometries along the minimum energy path have been illustrated in the insets.

only B_2 is dissociated back into individual boron atoms while BN is more persistent.

D. Further development of graphitic BN

As mentioned in earlier sections, the adsorption geometry BN-1 (see Fig. 4) seems to be an attractive intermediate step for graphitic BN formation; the BN molecule is situated above the topmost Mg(0001) layer and, although not calculated in this work, we can speculate that the migration barrier for a BN molecule between neighboring sites in the BN-1 geometry is not that big; the molecule-substrate interactions are rather weak (as described by the PDOS plots) and the molecule is above the topmost surface layer. The migration barrier from BN-1 to BN-2 was also seen to be reasonably small (0.56 eV), so if BN molecules are formed below the topmost Mg(0001) layer (BN-2), they can easily migrate above the surface (BN-1).

In realistic temperatures and pressures, graphitic-sheet formation can, of course, be a very complicated process. In this work and limited by the computationally demanding *ab initio* methods, we are interested in a theoretical "best case scenario," i.e., does the catalyst surface allow for further BN nucleation if we put several BN molecules on the surface and in the most suggestive adsorption geometries? In order to test this, we have adsorbed BN molecules in the BN-1 geometry on a $5\times5\times4$ Mg(0001) slab. The initial and final situations are illustrated in Fig. 11 and after ~2000 conjugate gradient relaxation steps one can observe the formation of several new BN bonds.

V. DISCUSSION

In this work we studied the elemental boron and nitrogen chemistry on a magnesium substrate. It was motivated by the state of the art method for producing BNNTs, where liquid magnesium droplets have been speculated to act as catalysts[7,12,13,19] in the reduction in boric oxide and ammonia into boron nitride nanotubes. We studied individual boron and nitrogen atoms on magnesium as well as elemental reactions forming the smallest molecules from these species, namely, N_2, B_2 and BN. Our study concentrated on the interaction of these species at a low concentration and in the absence of any defects or low-coordinated surface sites. Although it is very difficult to draw general conclusions about the actual synthesis method based on this simplified DFT study, we obtained some indications how boron-nitride nucleation could be promoted by magnesium.

Both boron and nitrogen were seen to favor the Mg(0001) octahedral site. Nitrogen was seen to accommodate also the Mg(0001) tetrahedral (metastable) site. As these two sites are next to each other, they provide a natural "template" for BN molecule formation, i.e., B can occupy the octahedral (B-1) site while N may occupy the neighboring metastable tetrahedral (N-2) site. This way both B and N can occupy a (meta-) stable site while still forming a BN molecule. From the adsorption geometry formed this way (BN-2) the BN molecule can migrate to another, energetically even more stable adsorption site that resides above the topmost magnesium layer. This new adsorption geometry (BN-1) has a rather weak interaction with the magnesium substrate and is a likely promoter of further BN nucleation. The case of the B_2 molecule was seen to be very different when compared to the BN molecule; B_2 does not adsorb above the surface, and from the PDOS we could see that its interaction with magnesium is rather strong. It also binds to the substrate using the low-

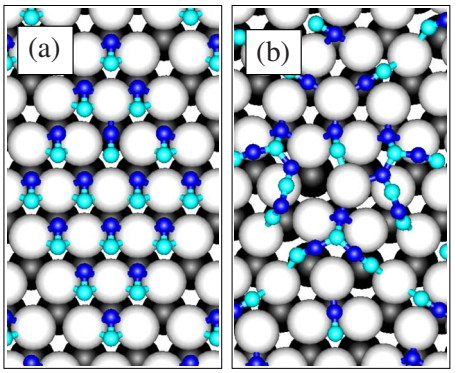

FIG. 11. (Color online) Relaxation of BN molecules placed on the magnesium surface in the BN-1 adsorption geometry.

lying σ_s^* molecular orbital and this might be a factor destabilizing the molecule (when compared to BN).

The competing reactions $B^*+B^* \rightarrow B_2^*$ and $B^*+N^* \rightarrow BN^*$ were seen to have almost equal reaction energies, within the limit of our computational accuracy. Both reactions were seen to be energetically favorable and there also seems to be an energy gain in bringing individual B and N atoms into nearby adsorption sites. The barriers for association/dissociation reactions of the smallest molecules indicate that B_2 dissociates easier while BN seems to be harder to break apart into individual atoms once it has been formed (although the differences between activation energies are quite small).

Summarizing, the interpretation that magnesium catalyst droplets act as catalysts in BNNT production[7,12,13,19] is tentatively supported by our calculations. This is in stark contrast to iron, where the flat bcc(110) surface was shown to disfavor BN molecule formation.[8] In the future, and if the interpretation of the experimental synthesis method becomes more clear, it might be interesting to study the stability of the precursors (boric oxide and ammonia) on a magnesium catalyst, as well as bulk diffusion and other phenomena involved in the synthesis method.

ACKNOWLEDGMENTS

We wish to thank the Center for Scientific Computing Helsinki, for use of its computational resources. This work has been supported in part by the European Commission under the 6 Framework Programme (STREP project BNC Tubes, Contract No. NMP4-CT-2006-03350) and the Academy of Finland through its Centre of Excellence program (Grant No. 2006-2011). S.R. acknowledges useful discussions with Dmitri Golberg.

*sampsa.riikonen@iki.fi

[1] N. G. Chopra, R. J. Luyken, K. Cherrey, V. H. Crespi, M. L. Cohen, S. G. Louie, and A. Zettl, Science **269**, 966 (1995).
[2] D. Golberg, Y. Bando, M. Eremets, K. Takemura, K. Kurashima, and H. Yusa, Appl. Phys. Lett. **69**, 2045 (1996).
[3] A. Rubio, J. L. Corkill, and M. L. Cohen, Phys. Rev. B **49**, 5081 (1994).
[4] X. Blase, A. Rubio, S. G. Louie, and M. L. Cohen, Europhys. Lett. **28**, 335 (1994).
[5] J.-C. Charlier, A. De Vita, X. Blase, and R. Car, Science **275**, 647 (1997).
[6] H. Tokoro, S. Fujii, and T. Oku, Diamond Relat. Mater. **13**, 1139 (2004).
[7] D. Golberg, Y. Bando, C. Tang, and C. Zhi, Adv. Mater. **19**, 2413 (2007).
[8] S. Riikonen, A. S. Foster, A. V. Krasheninnikov, and R. M. Nieminen, Phys. Rev. B **80**, 155429 (2009).
[9] P. Gleize, M. C. Schouler, P. Gadelle, and M. Caillet, J. Mater. Sci. **29**, 1575 (1994).
[10] K. F. Huo, Z. Hu, F. Chen, J. J. Fu, Y. Chen, B. H. Liu, J. Ding, Z. L. Dong, and T. White, Appl. Phys. Lett. **80**, 3611 (2002).
[11] J. J. Fu, Y. N. Lu, H. Xu, K. F. Huo, X. Z. Wang, L. Li, Z. Hu, and Y. Chen, Nanotechnology **15**, 727 (2004).
[12] C. Tang, Y. Bando, T. Sato, and K. Kurashima, Chem. Commun. **2002**, 1290.
[13] C. Zhi, Y. Bando, C. Tan, and D. Golberg, Solid State Commun. **135**, 67 (2005).
[14] J. K. Nørskov, A. Houmøller, P. K. Johansson, and B. I. Lundqvist, Phys. Rev. Lett. **46**, 257 (1981).
[15] T. Vegge, Phys. Rev. B **70**, 035412 (2004).
[16] Y. Li, P. Zhang, B. Sun, Y. Yang, and Y. Wei, J. Chem. Phys. **131**, 034706 (2009).
[17] M. Pozzo and D. Alfe, J. Phys.: Condens. Matter **21**, 095004 (2009).
[18] A. W. Searcy and C. E. Myers, J. Phys. Chem. **61**, 957 (1957).
[19] T. Terao, Y. Bando, M. Mitome, K. Kurashima, C. Zhi, C. Tang, and D. Golberg, Physica E (Amsterdam) **40**, 2551 (2007).
[20] Dmitri Golberg (private communication).
[21] C. Tang, Y. Bando, and T. Sato, Chem. Phys. Lett. **362**, 185 (2002).
[22] Facility for analysis of chemical thermodynamics (fact), http://www.crct.polymtl.ca/fact/
[23] J. M. Soler, E. Artacho, J. D. Gale, A. García, J. Junquera, P. Ordejón, and D. Sánchez-Portal, J. Phys.: Condens. Matter **14**, 2745 (2002).
[24] D. Sánchez-Portal, P. Ordejón, E. Artacho, and J. M. Soler, Int. J. Quantum Chem. **65**, 453 (1997).
[25] G. Kresse and J. Hafner, Phys. Rev. B **47**, 558 (1993).
[26] G. Kresse and J. Furthmüller, Phys. Rev. B **54**, 11169 (1996).
[27] G. Kresse and D. Joubert, Phys. Rev. B **59**, 1758 (1999).
[28] P. E. Blöchl, Phys. Rev. B **50**, 17953 (1994).
[29] J. P. Perdew, K. Burke, and M. Ernzerhof, Phys. Rev. Lett. **77**, 3865 (1996).
[30] Y. Zhang and W. Yang, Phys. Rev. Lett. **80**, 890 (1998).
[31] H. J. Monkhorst and J. D. Pack, Phys. Rev. B **13**, 5188 (1976).
[32] M. Methfessel and A. T. Paxton, Phys. Rev. B **40**, 3616 (1989).
[33] G. Henkelman, B. P. Uberuaga, and H. Jónsson, J. Chem. Phys. **113**, 9901 (2000).
[34] webelements.com, http://www.webelements.com
[35] A. Leonardo, I. Y. Sklyadneva, V. M. Silkin, P. M. Echenique, and E. V. Chulkov, Phys. Rev. B **76**, 035404 (2007).
[36] E. Wachowicz and A. Kiejna, J. Phys.: Condens. Matter **13**, 10767 (2001).
[37] P. Staikov and T. S. Rahman, Phys. Rev. B **60**, 15613 (1999).
[38] E. V. Chulkov and V. M. Silkin, Solid State Commun. **58**, 273 (1986).
[39] F. Schiller, R. Keyling, E. V. Chulkov, and J. E. Ortega, Phys. Rev. Lett. **95**, 126402 (2005).
[40] B. Hammer, Top. Catal. **37**, 3 (2006).
[41] B. Hammer, L. B. Hansen, and J. K. Nørskov, Phys. Rev. B **59**, 7413 (1999).
[42] B. Hammer and J. K. Nørskov, Surf. Sci. **343**, 211 (1995).